Proceedings of the 17th Pan-American Conference on Soil Mechanics and Geotechnical Engineering (XVII PCSMGE), and 2nd Latin-American Regional Conference of the International Association for Engineering Geology and the Environment (IAEG), La Serena Chile, 2024.

Three-dimensional numerical simulation of tunneling in soft soils with TBM-EPB

Simulação numérica tridimensional da escavação de tuneis em solos moles com TBM-EPB

Juan Félix Rodríguez Rebolledo & Edwin Santos Colque
Postgraduate Program in Geotechnics, University of Brasilia (UnB), Brazil, jrodriguezr72@unb.br

Gabriel Auvinet
Engineering Institute, National University of Mexico (UNAM), Mexico

ABSTRACT: In this article, the methodology employed to define a model using the Finite Element Method (FEM, Plaxis 3D) for simulating the excavation of a tunnel with TBM-EPB is presented. The model considers a representative stratigraphy of the Mexico City lacustrine zone and considers the specific characteristics of the Tunel Emisor Oriente (TEO). Additionally, Soft Soil Creep (SSC) constitutive model is utilized. The article begins by outlining the characteristics of the reference model, followed by a description of the constitutive models used and the defined obtained and adjusted parameters. Finally, all the steps involved in developing the numerical modeling are detailed. The results obtained highlight the limitations of the Tunnel Designer module of the Plaxis 3D software and suggest potential adjustments for a more realistic modeling of tunnel construction using TBM-EPB in these difficult subsoil conditions.

KEYWORDS: Finite Element Method, 3D model, Tunel Emisor Oriente, Soft Soil Creep model, TBM-EPB.

1 INTRODUCTION.

The expansion of urban areas, both in terms of population and geographic coverage, has created an increasing demand for the implementation of new infrastructure. This includes systems related to public transportation and drainage, which are essential elements that must be located underground due to the limited surface space in densely populated urban areas.

The challenging conditions presented by the lake soils of Mexico City, characterized by highly plastic clays of volcanic origin with high water content reaching up to 400%, significant compressibility, and pore water pressure drawdown conditions, necessitate the utilization of advanced technology for large tunnel excavation. Specifically, the use of Tunnel Boring Machines (TBMs) of the Earth Pressure Balance (EPB) type has proven crucial in minimizing the likelihood of surpassing ultimate limit states of failure and serviceability for both the excavated tunnel and surrounding structures.

Numerical simulation has emerged as a versatile and invaluable tool in the realm of underground construction, where the subsoil can be treated as a continuous medium, allowing for the adaptation of simplified models to real-world scenarios (Assis 2002). The excavation of tunnels in soft soils often involves the use of Earth Pressure Balance (EPB) tunnel boring machines, which apply pressure on the excavation face using the excavated material itself (Chapman *et al*., 2018). In numerical simulations of TBM-EPB operations, it is crucial to accurately portray the construction process, including the pressure exerted on the excavation face, the contraction resulting from the tunnel shield's conical shape, the forward force from hydraulic jacks, and the grout pressure into the annular space left by the shield tail (Auvinet *et al.*, 2017).

Numerous studies in the literature have evaluated the deformations induced by TBM-EPB during tunnel excavation and potential control mechanisms to minimize these effects. Notable works include those by Mair and Taylor (1997), Sugiyama *et al.* (1999), Lee *et al.* (2000), Wongsaroj *et al.* (2006), Gens *et al.* (2009), Michael *et al.* (2017), Chapman *et al.* (2018), Jallow et al. (2019), Ling *et al.* (2022), among others.

With 62 km in length, the *Emisor Oriente* Tunnel (TEO) in Mexico City is considered one of the largest of its kind in the world. Its construction began in 2009, and it started operating at full capacity in 2020. It was constructed using EPB type tunnel boring machines. The initial segment of the tunnel traverses the compressible clays of the lacustrine zone for its first few kilometers. According to the findings from the instrumentation in this segment, Aguilar-Tellez *et al.* (2012) reported convergence values of the segmented lining ranging from 4 to 5.5 cm, reaching up to 7 cm, and surface subsidence values ranging from 4.4 to 14.3 cm. Similarly, Hernández (2013) presented average convergence values of 4 to 8 cm, with occasional peaks reaching up to 18 cm.

As part of a collaborative project between the University of Brasilia (UnB) and the Engineering Institute of the National Autonomous University of Mexico (UNAM), research is being conducted with the overarching aim of performing a three-dimensional parametric analysis. This analysis seeks to facilitate an understanding of the primary variables influencing convergences and surface settlements when constructing a tunnel through the lacustrine clays of Mexico City using TBM-EPB. The parameters under scrutiny include clay stiffness, segmented lining stiffness, grout pressure, excavation face pressure, excavation speed, drainage condition, and piezometric conditions.

This article outlines the methodology employed to establish a numerical model based on the three-dimensional Finite Element Method (FEM, Plaxis 3D) for simulating the excavation of a tunnel with TBM-EPB through a representative stratigraphy of the Mexico City lacustrine zone. The model takes into account the dimensions and characteristics of the TEO while utilizing the Soft Soil Creep (SSC) constitutive model.

The initial section of the article introduces the definition and features of the reference model, encompassing the tunnel's characteristics, TBM specifications, and the pertinent stratigraphy. Subsequently, a general overview of the constitutive models utilized is provided, along with the definition of parameters obtained and adjusted through laboratory tests. The article comprehensively describes all stages involved in developing the numerical model, including: 1) model dimensions and boundary conditions, 2) TBM-EPB simulation, 3) analysis stages, and 4) measurement sections. Finally, the article presents results pertaining to vertical displacements during TBM excavation progress and convergences obtained for various values of the reduction factor of the flexural rigidity of the lining (α).

The obtained results highlight the limitations of the Tunnel Designer module within the Plaxis 3D software and suggest potential adjustments for a more realistic modeling of tunnel construction using TBM-EPB in difficult subsoil conditions.

2 REFERENCE MODEL

2.1 *Characteristics of the tunnel and the TBM-EPB*

For this study, the characteristics and dimensions of the TEO were taken into account (see Figure 1), with a finished internal diameter of 7 m and excavation carried out using a TBM of EPB type. Prefabricated segmented rings, 35 cm thick and 1.5 m wide, were utilized as the primary lining, followed by an additional cast-in-place final lining of the same thickness, consisting of a continuous ring of reinforced concrete.

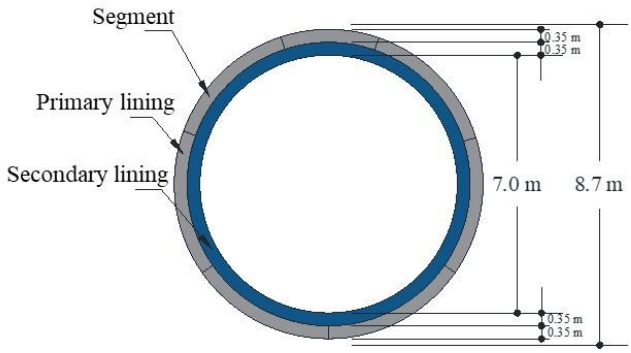

Figure 1. Geometry of the tunnel.

In this study, focus was placed solely on the primary lining, as the analysis was conducted for the tunnel excavation stage, with the final lining being installed one year subsequent to this stage.

The TBM features a cutterhead with an approximate diameter of 8.7 m and a slightly conical shield measuring 9 m in length, including a 1.5 m tail. This equipment is capable of exerting pressure at the front to maintain stability, aided by a screw conveyor for mud pressure control and hydraulic jacks that propel the TBM forward, reacting with the already installed segment lining. The segmented ring is constructed on the shield's tail, and upon advancing 1.5 m, it establishes contact with the ground through an injection of approximately 15 cm thick mortar.

For the subsequent analyses presented, it was essential to define the total weight of the shield and the forward speed. The estimated weight of the shield, including the cutterhead, was approximately 3.3 MN (Ríos, 2009). The forward speed was determined based on field records: maximum speed of 31 m/day, average of 163 m/week, and a minimum of 592 m/month.

2.2 *Soil and stratigraphic conditions*

The aim was to represent the typical stratigraphic conditions of the lacustrine zone in Mexico City, given the extensive tunnel network, which includes those belonging to the deep drainage system and subway, that has been excavated through the Upper Clay Formation. Additionally, for the tunnel to be classified as deep, the tunnel crown was situated at a depth three times the internal diameter (21m). To ensure that it was not affected by the rigidity and strength of the underlying hard layer, a vertical distance of twice the internal diameter (14m) from the tunnel invert was considered. Figure 2 illustrates the stratigraphy used in this study.

The water table was assumed to be 3m deep, aligning with the lower boundary of the surface crust. The mechanical and hydraulic properties of the Surface Crust and clay formations were estimated based on the findings of Rodríguez *et al.* (2012) and Alberro and Hiriart (1973).

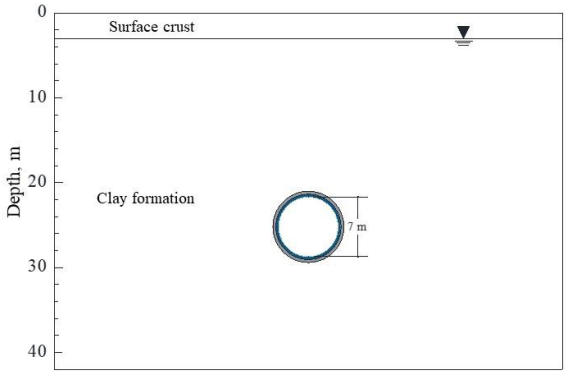

Figure 2. Considered stratigraphic conditions.

3 CONSTITUTIVE MODELS

The constitutive models employed in the numerical simulation were as follows:

1) The Linear Elastic (LE) model was utilized to characterize the mechanical response of the primary lining and the shield of the TBM.

2) The Mohr-Coulomb (MC) model was employed to replicate the behavior of the superficial crust.

3) Lastly, the Soft Soil Creep (SSC) model was applied to simulate the behavior of lacustrine clays.

3.1 *Mohr-Coulomb (MC) model*

This simplified model was employed to simulate the Surface Crust behavior, as it is anticipated that this layer has minimal influence

on the tunnel's behavior. Additionally, due to its highly preconsolidated nature, employing constitutive models based on critical state theory would be unsuitable.

The properties attributed to the Surface Crust are outlined in Table 1.

Table 1. Considered parameters for the Surface Crust.

Model	*w* (%)	γ (kN/m³)	E' (MPa)	ν'	c' (MPa)	φ' (°)	ψ (°)	K_o
MC	33	14	5	0.30	20	40	0	1.00

w = water content; γ = unit weight; E' = drained Young modulus; c' = effective cohesion; φ' = effective friction angle; ν' = drained Poisson´s ratio; ψ = dilatancy angle; K_o= coefficient of earth pressure at rest; MC = Mohr-Coulomb model.

3.2 *Soft Soil Creep (SSC) model*

The SSC model is an extension of the Soft Soil model, which is based on the Cam-Clay model originally developed at the University of Delft in the Netherlands and subsequently incorporated into the Plaxis software.

Similar to the Cam-Clay model, the SSC model assumes isotropic elastic behavior, defined by the parameters *K* (volumetric stiffness modulus) and *G* (shear stiffness modulus). In the case of the SSC model, the increase in volumetric elastic strain (ε_p^e) is determined using the average value of the modified swelling index (κ^*). The yield surface takes on an elliptical shape but does not intersect the origin; its size and shape are characterized by parameters *c*, ϕ, M^*, and p_0. The failure criterion is based on the MC model and is independent of the yield surface. Volumetric hardening, i.e., the expansion of the yield surface, is contingent upon isotropic plastic deformations, which in turn depend on the average value of the modified compression index (λ^*), the modified creep index (μ^*), and time.

The SSC model was selected to simulate the behavior of lacustrine clays due to its capability to account for the material's response based on the excavation speed of the tunnel boring machine, under both drained and undrained conditions.

3.3 *Obtaining and adjusting parameters*

The strength and compressibility parameters for the SSC model were derived from CU (undrained isotropic consolidation) and CD (drained isotropic consolidation) triaxial tests conducted by Alberro and Hiriart (1973) on an undisturbed sample of lacustrine clay at a depth of 2.5 m, with an initial water content of 293% (i.e., e_0 = 10.18).

The CU tests were performed at axial strain rates ($\dot{\varepsilon}$) of 94, 1.88, and 0.045 %/hour, and at confining stresses (σ_3) of 25, 50, and 100 kPa. Figure 3 illustrates the stress trajectories obtained and the inclination of the critical state line (*M*) as part of the analyses, where the isotropic stress is $p = (\sigma_1 + 2\sigma_3)/3$ and the deviatory stress is $q = \sigma_1 - \sigma_3$.

The parameters derived from the triaxial tests were adjusted using the SoilTest module of the Plaxis software, with comparisons made between simulation and laboratory tests results. Stress trajectories for the CU (Figure 4) and CD tests, as well as the axial strain versus deviatoric stress curves ($\varepsilon_1 - q$) and axial strain versus pore water pressure curves ($\varepsilon_1 - u$), were compared. As depicted in Figures 3 and 4, the fit achieved was satisfactory, demonstrating the model's capacity to replicate the influence of load application speed on effective stresses and pore water pressure. The calibrated parameters for the SSC model are summarized in Table 2.

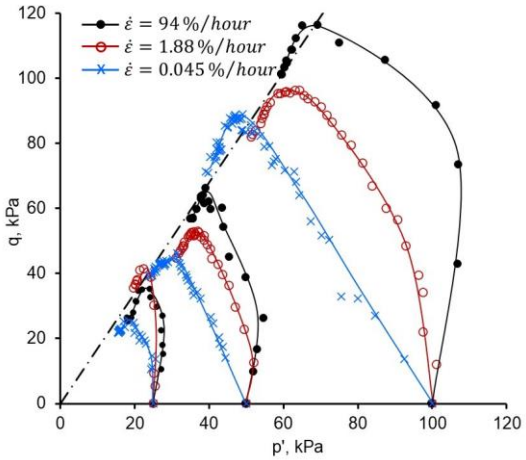

Figure 3. Stress trajectories and inclination of the critical state line obtained from CU triaxial test at confining stresses (σ_3) of 25, 50, and 100 kPa and axial strain rates ($\dot{\varepsilon}$) of 94, 1.88, and 0.045 %/hour.

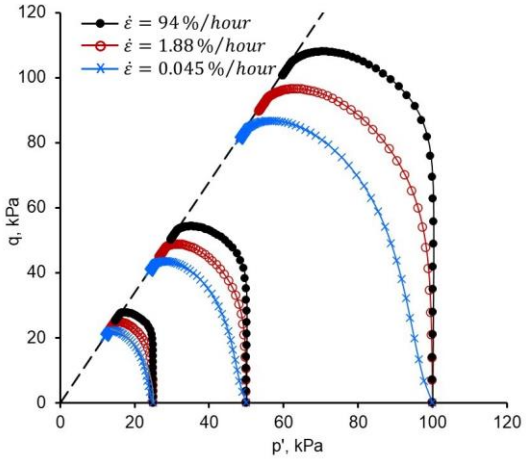

Figure 4. Stress trajectories and inclination of the critical state line obtained from numerical modelling (SoilTest module) using SSC model.

Table 2. Obtained and calibrated parameters for the SSC model.

γ kN/m³	κ^*	λ^*	μ^*	*OCR*	c' MPa	φ' °	ν_{ur}	K_o^{nc}
11.6	0.04	0.35	0.01	1.0	0	42	0.30	0.48

γ = unit weight, κ^* modified swelling index, λ^* = modified compression index, μ^* = modified creep index; *OCR* = over-consolidation ratio, c' = effective cohesion, φ' = effective friction angle, ν_{ur} = Poisson's ratio for unloading-reloading; K_0^{nc} = effective stress ratio in a state of normal consolidation.

For the superficial crust, a permeability value ($k_x = k_y = k_z$) of $1x10^{-2}$ m/day was considered, and for the upper clay series of $1x10^{-5}$ m/day, both values were obtained from Rodríguez *et al.* (2012).

4 NUMERICAL MODEL

4.1 *General characteristics of the software*

The numerical simulation utilized Plaxis 3D (Connect Edition, version 21), which is based on the finite element method (FEM, Bentley 2021). The medium was discretized using a mesh composed of tetrahedral elements with ten nodes and four stress integration points. Additionally, plate-type elements consisting of triangular elements with six nodal points and three stress points, along with interface elements comprising six pairs of nodes, were employed.

4.2 *Dimensions of the model and boundary conditions*

To define the model's dimensions, the Möller's (2006) recommendations were adopted, as shown in Figure 5. Condition of symmetry were considered, thus only the half of the tunnel was modeled. Displacements at the lateral boundaries were restricted in the horizontal axes (X and Y) and left free in the vertical direction (Z). At the lower boundary, which is limited by the depth of the hard layer, displacements were restricted in all directions (X, Y, and Z). The upper boundary was entirely unrestricted. As for the consolidation of the medium, water flow was permitted only through the upper and lower borders of the model, assuming that the lower boundary comprises a hard layer with considerably higher permeability than clay.

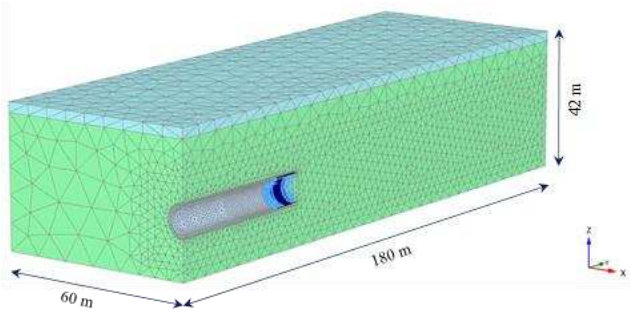

Figure 5. Finite element mesh.

The medium was discretized using a total of 36,372 tetrahedral elements and 57,119 nodes. A mesh refinement was performed around the tunnel construction zone (one time the tunnel diameter) with a densification factor of 0.3. Mesh sensitivity analyses were conducted to ensure that the model's dimensions and the element density employed were the minimum required to avoid influencing the obtained results.

4.3 *TBM-EPB simulation*

The overall dimensions of the TBM-EPB shield and the magnitudes of the operating pressures considered for numerical modeling are depicted in Figure 6. In order to simplify the model, the annular space of 15 cm of grout around the segments was not taken into account, resulting in an excavation diameter of 8.4 m.

The operating pressure at the face (214.0 to 331.7 kPa) was calculated based on criteria defined by Kanayasu *et al.* (1994), Mollon *et al.* (2012), and Lee *et al.* (2021), considering the initial total horizontal stress developed at the machine face depth. The injection pressure (251.0 to 344.4 kPa) was determined from the initial total vertical stress developed around the shield in the tail area. The thrust pressure (811 kPa), generated by the hydraulic jacks, was derived from the total force magnitude generated by the face pressure and the cross-sectional area of the segmented ring. A soil contraction around the shield of approximately 4 cm was considered due to its conical shape, progressively occurring from the cutting head to the start of the tail (8.4 m).

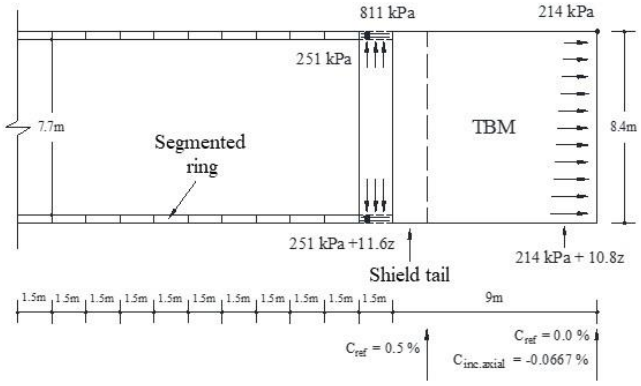

Figure 6. TBM-EPB dimensions.

The segments were simulated using tetrahedral elements, and the tunnel boring machine's shield with plate elements, considering a linear elastic behavior for both. Their properties are presented in Table 3.

Table 3. Lining and shield properties.

Elements	Thickness (m)	γ (kN/m³)	E (GPa)	ν	α
Segment	0.35	24	5.2	0.15	0.2
Shield	0.17	78.6	200	-	-

γ = unit weight, E = Young modulus, ν = Poisson's ratio, α = reduction factor for bending stiffness.

To account for the effect of the joints between the segments on the ring's bending stiffness, Rodríguez et al. (2012) propose the use of a stiffness reduction factor denoted as α, on the order of 0.2. It is important to note that this factor was calculated for plane strain analyses and, according to Auvinet et al. (2017), there is evidence that its value is not independent of the pressure conditions around the tunnel and tends to decrease drastically when there is significant stress deviation.

The shield thickness (Table 3) was calculated based on its weight (approximately 330 t) and the steel's volumetric weight. The steel's modulus was considered for E.

For the TBM simulation, the software includes a module called Tunnel Designer (Figure 7). This module allows for defining the shape and dimensions of the excavation, dimensions and properties of the primary lining and shield, operating pressures (face, grout, and jacks, Figure 8), soil convergence, and excavation sequence.

Table 4 presents the sequence for the TBM simulation, with an excavation progress of 1.5 m for each sequence. Sequences 1 to 6 simulate material cutting and shield advancement (plate elements). In the first sequence, face pressure is applied along with the initial soil convergence increment (0.0667%/m), and from sequences 2 to 5, subsequent increments are applied up to a total convergence of 0.5% (4.2 cm). Sequence 6 simulates the passage of the tail, and in sequence 7, grout pressure is directly applied to the soil. Finally, in

sequence 8, the segmented ring is placed (tetrahedral concrete element), and jacks pressure is applied.

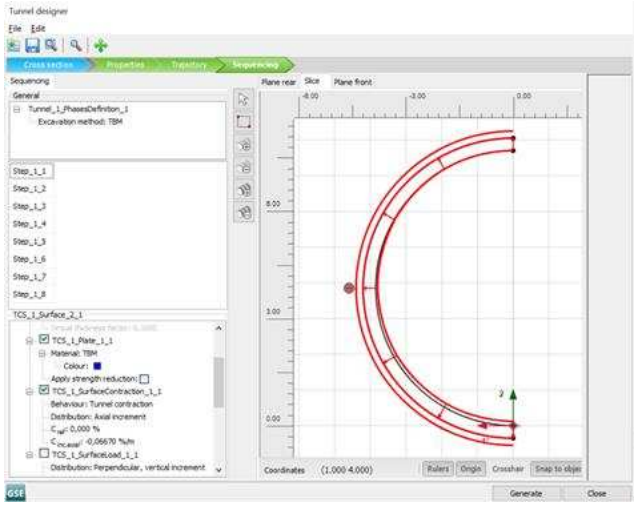

Figure 7. Tunnel Designer module for TBM simulation.

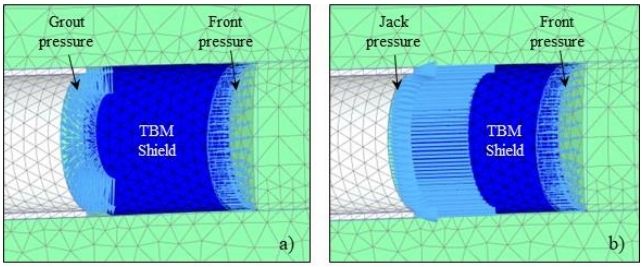

Figure 8. a) Front and grout pressures (Sequence 7, 10.5 m progress) and b) front and jack pressures (Sequence 8, 12 m progress).

4.4 *Analysis stages*

The analysis stages were as follows:

Initial Stage: Initial stresses are generated in the medium using the K_0 procedure.

Stage 1: The initial position of the TBM is defined. To avoid the influence of boundary conditions, it is assumed that the first 25 m of the tunnel have already been constructed. In other words, the soil inside the tunnel (excavation) is deactivated, and the elements of the segmented lining are activated. The shield is positioned from 26.5 to 35.5 m of excavation progress, activating sequences 1 to 7 (Table 4).

Stage 2: The shield advances 1.5 m (from 28 to 37 m), and the first segmented ring is installed, activating sequences 1 to 8 (Table 4).

Stage 3: The displacements obtained in the previous stages are reset using the "reset displacements" function, and TBM advances 1.5 m (from 29.5 to 38.5 m). Sequences 1 to 8 are activated (Table 4) during this stage. From this point onward, the convergence of the lining is measured.

Stages 4 to 11: The TBM advances 1.5 m for each stage, activating sequences 1 to 8 for each one. This continues until the excavation face reaches 50.5 m, completing an overall excavation progress of 13.5 m from Stage 3.

Table 4. Excavation sequence.

Seq.	Progress	Element	Contraction	Applied pressures
1	1.5 m	Shield	C_{ref}: 0,00% $C_{inc.axial}$:-0,0667%m	$\sigma_{n,ref}$: -214 kPa $\sigma_{n,inc}$: -10.8 kPa/m z_{ref}: -21 m
2	3.0 m	Shield	C_{ref}: 0,10% $C_{inc.axial}$:-0,0667%m	-
3	4.5 m	Shield	C_{ref}: 0,20% $C_{inc.axial}$:-0,0667%m	-
4	6.0 m	Shield	C_{ref}: 0,30% $C_{inc.axial}$:-0,0667%m	-
5	7.5 m	Shield	C_{ref}: 0,40% $C_{inc.axial}$:-0,0667%m	-
6	9.0 m	Shield	C_{ref}: 0,50%	-
7	10.5 m	-	-	$\sigma_{n,ref:}$ -251 kPa $\sigma_{n,inc:}$ -11.6 kPa/m z_{ref}: -21 m
8	12,0 m	Segment	-	$\sigma_{n,ref}$: 811 kPa

C_{ref} = reference contraction, $C_{inc.axial}$ = contraction axial increment, $\sigma_{n,ref}$ = reference pressure, $\sigma_{n,inc}$ = pressure increment, z_{ref} = reference depth.

Sensitivity studies conducted up to 20 analysis stages revealed that the convergences in the segmented lining stabilized after a 13.5-meter progress, measured from Stage 3. This finding enabled to conclude that simulations only needed to extend up to Stage 11, leading to a substantial reduction in analysis time.

All stages were simulated under undrained conditions, considering an average construction rate of 15.5 segments/day (0.0644 days/segment).

4.5 *Measurement Sections*

To maximize the utility of results obtained from each analysis, three measurement sections were defined along the excavation sequence, as illustrated in Figure 9. The following points were established:

Points A1 and B1: These points were designated to determine displacements and stresses resulting from the approach of the excavation face (steps 1 to 8, corresponding to Stages 3 to 10, covering a 12-m excavation progress).

Points A2 and B2: These points were used to assess displacements and induced stresses during the shield passage (steps 9 to 15, corresponding to Stages 3 to 9, covering a 10.5-m excavation progress).

Points A3 and B3: These points allowed measurement of displacements and stresses within the segmented lining as the tunnel boring machine moved away (steps 16 to 24, corresponding to Stages 3 to 11, covering a 13.5-m excavation progress). This cumulative relative progress totaled 36 m, with simulations conducted for only 11 analysis stages.

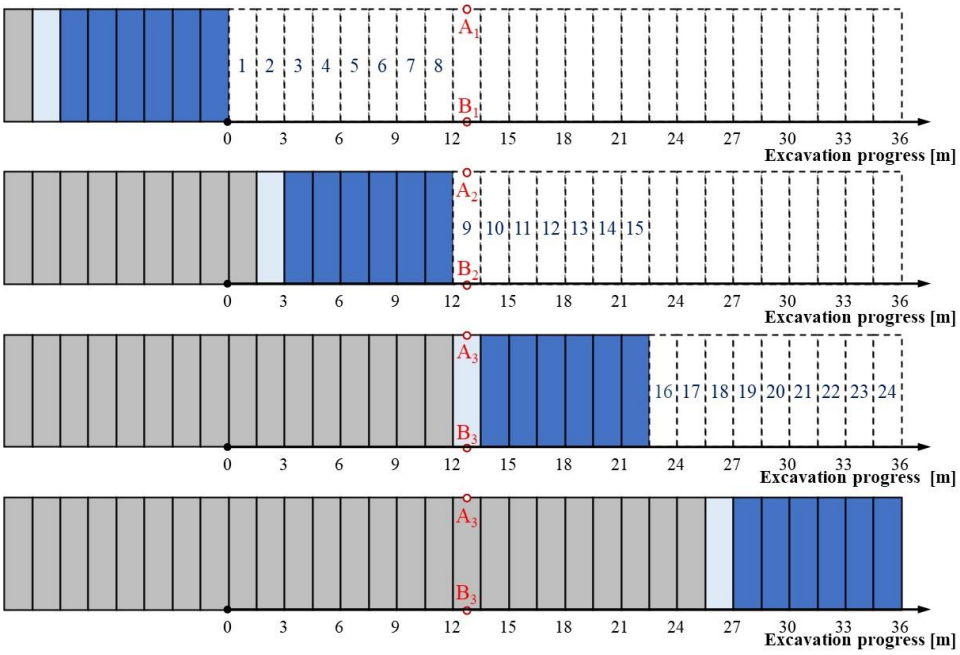

Figure 9. Excavation sequences and measurement sections.

Point A was positioned at a depth of 21 meters at the tunnel crown, while Point B was located in the invert at a depth of 29.4 meters.

5 RESULTS AND DISCUSSIONS

5.1 *Vertical displacements*

Vertical displacements and convergences induced by tunnel construction at Points A and B were determined throughout the approach, passage, and withdrawal of the TBM shield, as described in the preceding sections.

Figure 10 illustrates the vertical displacements obtained. Remarkably, displacements begin to occur even during the TBM's approach (excavation progress from 0 to 12 m), with nearly equal magnitudes at both points (virtually negligible vertical convergence, as depicted in Figure 11). This behavior signifies an upward movement of the excavation, intensifying significantly during the TBM's passage and withdrawal, with more pronounced effects observed at the invert (Point B) compared to the crown (Point A). This phenomenon, previously observed by Auvinet and Rodríguez (2010) and Zaldivar *et al.* (2012) during simulations for the definitive lining design of the TEO, is commonly referred to as the "bubble effect." Essentially, the discharge resulting from the removal of excavated soil weight leads to an overall upward movement of the tunnel, altering stress and displacement conditions in the surrounding soil.

During the TBM's passage (excavation progress from 12 to 21 m), Point B experiences greater discharge than Point A due to the contraction effect under consideration. Specifically, while the contraction effect contributes to the discharge at Point B, the opposite effect is observed at Point A. This behavior is evident in the vertical convergences (Figure 11): upon reaching the excavation face, a 5 mm convergence is observed, which increases to 52 mm as the shield passes, resulting in a 47 mm increment during the shield's passage. Consequently, the shield itself experienced a convergence of approximately 5 mm, considering the assumed contraction value of 42 mm.

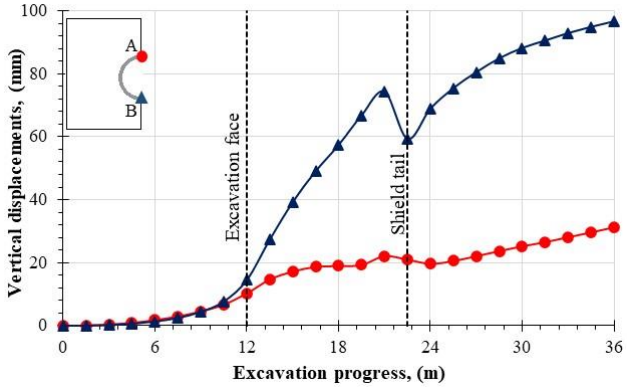

Figure 10. Vertical displacements during tunnel excavation.

Between 24 and 36 m of excavation progress, the vertical displacements and convergences correspond to the condition where the soil comes into contact with the segmented lining. Notably, in Figure 10 at Point A, the "bubble effect" becomes apparent within this interval, creating the illusion that the lining is ascending at an approximate rate of 1 mm per meter—an effect likely corrected by the TBM operator without conscious perception. Conversely, Figure 11 reveals that soil convergences

grow to approximately 65 mm and stabilize at this value. This behavior demonstrates the action of the segmented lining, which absorbs the loads transmitted by soil excavation, thereby stabilizing the tunnel walls.

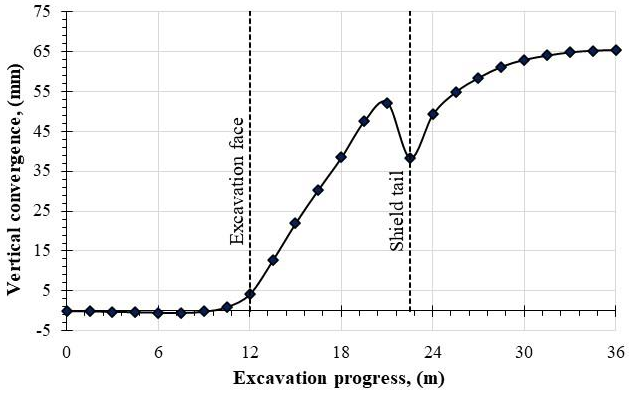

Figure 11. Vertical convergences during tunnel excavation.

5.2 *Primary lining convergence*

Convergence within the tunnel lining only begins to develop after its installation, specifically after an excavation progress of 24 m, as depicted in Figure 11. Consequently, it was necessary to reset the mesh displacements at Stage 3 of the analysis, as detailed in Section 4.4. In Figure 12, the vertical and horizontal convergences obtained within the segmental lining from its installation (0-m excavation progress) up to 13.5 m are illustrated. Notably, the maximum values reached were only 26 mm and 17 mm for vertical and horizontal convergence, respectively, as shown in Figures 12 and 13. These values are significantly below the average values reported by Téllez *et al.* (2012) and Hernández (2013) (ranging from 4 to 6 cm) for Section 1 of the TEO.

Based on the results obtained, it seems that the value of α (bending stiffness reduction factor, see Table 3) used for plane strain analysis is not appropriate for three-dimensional analysis since it does not account for the impact of longitudinal joints between segments.

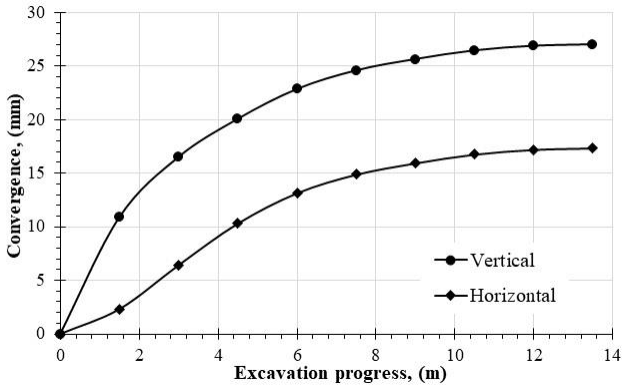

Figure 12. Primary lining convergences.

5.3 *Influence of Parameter α*

Figure 14 displays the convergence values obtained for α = 0.2, 0.1, and 0.067. Vertical convergences reach 40 mm and 50 mm for α values of 0.1 and 0.067, respectively. Consequently, α = 0.067 seems to correspond with the measured convergence values.

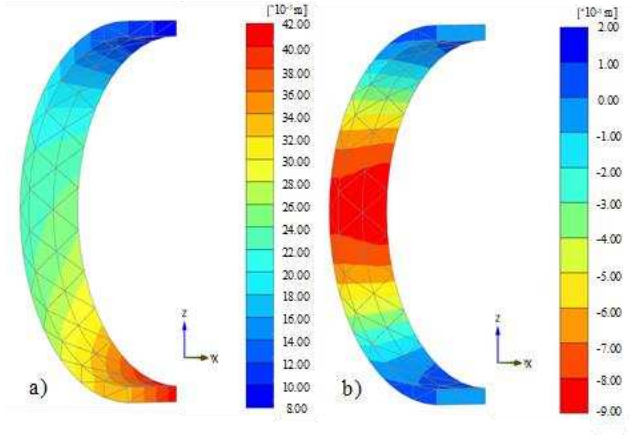

Figure 13. Lining deformations, a) vertical, b) horizontal.

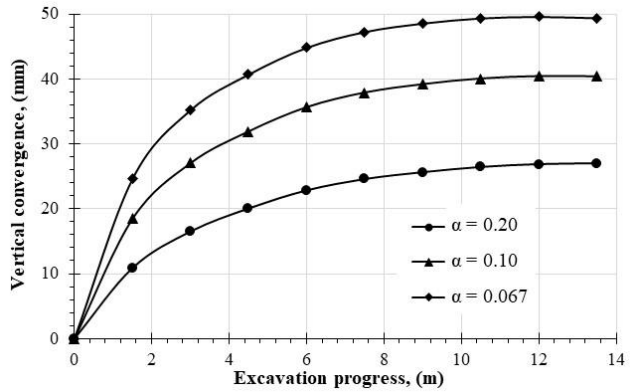

Figure 14. Variation of convergences in the primary lining for different values of α.

It is important to emphasize that the Tunnel Designer module of Plaxis does not address the potential effects on tunnel behavior resulting from transverse and longitudinal joints in the segmented lining in its tutorial. Disregarding the influence of these joints on the bending stiffness of the lining could result in an underestimation of convergences and even surface settlements during tunnel excavation.

6 CONCLUSIONS

This article presents a three-dimensional analysis of the excavation of a tunnel using an EPB (Earth Pressure Balance) TBM (Tunnel Boring Machine) in the lacustrine clays of Mexico City. The analysis was conducted using the three-dimensional finite element method (Plaxis 3D).

The behavior of soft soils was simulated using the Soft Soil Creep (SSC) constitutive model. The model parameters were

validated and adjusted based on CU triaxial laboratory tests conducted by Alberro and Hiriart (1973) at different strain rates.

The proposed methodology allowed to analyze the evolution of vertical displacements and convergences during the TBM's approach, passage, and withdrawal. Notably, the development of the "bubble effect" was observed during tunnel excavation and lining installation. This effect gives the appearance that the lining is ascending at an approximate rate of 1 mm/m. It is possible that the TBM operator corrects this effect without being noticed.

The stiffness of the segmental lining significantly influences convergence development. According to the obtained results, it appears that the value of α (bending stiffness reduction factor) adopted for plane strain analysis is not suitable for three-dimensional analysis, as it disregards the influence of longitudinal joints between segments. The analyses presented herein indicate that an α value of 0.067 would yield results closer to field measurements.

The obtained results highlight the limitations of Plaxis 3D's Tunnel Designer module and suggest adjustments for a more realistic modeling of tunnel construction using TBM-EPB in these challenging conditions.

7 ACKNOWLEDGEMENTS

The authors acknowledge the Coordination for the Improvement of Higher Education (CAPES) and the National Council for Scientific and Technological Development (CNPq) for their financial support and partnership.

8 REFERENCES

Aguilar M.A., Marroquín R.M., Rángel J.L, Comulada M. and Auvinet G. 2012. *Mexico City deep eastern drainage tunnel. Geotechnical Aspects of Underground Construction in Soft Ground*-Viggiani (ed), Taylor & Francis Group, London. pp. 3-20.

Alberro J. and Hiriart G. 1973. *Resistencia a Largo Plazo de las Arcillas de la Ciudad de México*. Instituto de Ingeniería UNAM, México. 77 p.

Auvinet G., Méndez E. and Juárez M. 2017. *El Subsuelo de la Ciudad de México*. Vol. 3, con revisión de avances, Universidad Nacional Autónoma de México, Instituto de Ingeniería UNAM, México. 335 p.

Assis, A.P. 2002. *Mecânica das Rochas: Obras Subterrâneas - Notas de Aula*. Departamento Engenharia Civil e Ambiental, Universidade de Brasília, Brasília, DF.

Bentley. 2021. Plaxis 3D: *Tutorial Manual*. Connect Edition V21.01. Dublin, Ireland.

Chapman, D., Metje, N. and Stärk, A. 2018. *Introduction to Tunnel Construction*. 2ª ed, Boca Raton: CRC Press, Boca Raton, USA. 425 p.

Gens, A., Persio, R., Di Mariano, A., Castellanza, R. and Arroyo, M. 2009. Relación entre parámetros de una tuneladora EPB y los movimientos del terreno. *Jornadas Hispano Portuguesas sobre geotecnia en las infraestructuras ferroviarias*, Madrid, pp. 433-441.

Hernández, R.G. 2013. *Instrumentación para la auscultación de túneles en suelos blandos*. Tesina de Especialidad en Geotecnia. UNAM, México. 85 p.

Jallow A., Ou Ch. and Lim A. 2019. Three-dimensional numerical study of long-term settlement induced in shield tunneling. *Tunnelling and Underground Space Technology* 88, pp. 221–236.

Lee, K.M., Ji, H.W., Shen, C.K., Liu, J.H. and Bai, T.H. 2000. A case study of ground control mechanisms of EPB shield tunneling in soft clay. *Proc. Int. Symposium on Geotechnical Aspects of Underground Construction in Soft Ground*, Tokyo, Balkema, pp. 251-256.

Lee H. Choi H., Chang S., Kang T. and Lee CH. 2021. Numerical Simulation of EPB Shield Tunneling with TBM Operational Condition Control Using Coupled DEM–FDM. *Applied Sciences* 11(6), 2551. 19 p.

Ling X., Kong X., Tang L., Zhao Y., Tang W. and Zhang Y. 2022. Predicting earth pressure balance (EPB) shield tunneling-induced ground settlement in compound strata using random forest. *Transportation Geotechnics* 35 (2022) 100771. 13p.

Maidl, B., Herrenknecht, M., Maidl, U. and Wehrmeyer, G. 2012. *Mechanised Shield Tunneling*. 2nd ed., Berlin: Ernst & Sohn, a Wiley Company, Berlin, Germany. 470 p.

Mair, R. J. and Taylor, R.N. 1997. Theme lecture: Bored tunneling in the urban environment. *Proc. 14th International Conference Soil Mechanicsand Foundation Engineering*, Hamburg, Balkema, Rotterdam, Vol. 4, pp. 2353-2385.

Michael K., Dimitris L., Ioannis V. and Petros F. 2017. Development of a 3D finite element model for shield EPB tunneling. *Tunneling and Underground Space Technology* 65, pp. 22–34.

Möller, S., 2006. *Tunnel induced settlements and structural forces in linings*. Herausgeber: Thesis doctoral Universitat Stuttgart. Institut für Getechnik. Herausgeber P. A. Vermeer, Berlin. 174 p.

Mollon G, Dias D. and Soubra A.H. 2012. Probabilistic analyses of tunnelling-induced ground movements. *Acta Geotechnica* 8. pp. 181-199.

Kanayasu S., Kubota I. and Shikubu N. 1995. *Stability of face during shield tunnelling – A survey on Japanese shield tunneling. in Underground Construction in Soft Ground*. Fujita & Kusakabe (eds), Balkema, Rotterdam. pp. 337-343.

Ríos A.M. 2009. *Procedimiento de excavación con escudo para la construcción del Túnel Emisor Oriente en el Valle de México*. Tesis. UNAM, México. 126 p.

Rodriguez J.F., Auvinet G., Aguilar M.A. and Pereyra J.A. 2012. Análisis y diseño del revestimiento definitivo de túneles en suelos blandos. *Proc. 2º Simposio Internacional sobre túneles y lumbreras en suelos y roca*. Mexico City. 10 p.

Sugiyama, T., Hagiwara, T., Nomoto, T., Nomoto, M., Ano, Y., Mair, R. J. and Soga, K. 1999. Observations of ground movements during tunnel construction by slurry shield method at the docklands light railway Lewisham Extension-East London. *Soils and Foundations*. Vol. 39. No 3. pp. 99-112.

Zaldivar, S.F., Rodríguez, J.F. and Auvinet, G. 2012. Esfuerzos y desplazamientos alrededor de un túnel considerando el "efecto burbuja". *Proc. 2° Simposio Internacional sobre túneles y lumbreras en suelos y roca*, SMIG, AMITOS, Mexico.